Impact of deformation on a supine-positioned image guided breast surgery approach

Winona L. Richey[a,b], Jon S. Heiselman[a,b], Ma Luo[a,b], Ingrid M. Meszoely[b,c], Michael I. Miga[a,b,d,e,f]

[a]Vanderbilt University, Department of Biomedical Engineering, 1225 Stevenson Center Ln, Nashville, USA, 37235
[b]Vanderbilt Institute for Surgery and Engineering, 1161 21st Ave. S., Nashville, USA, 37204
[c]Vanderbilt University Medical Center, Division of Surgical Oncology, 719 Thompson Ln Suite 22100, Nashville, USA, 37232
[d]Vanderbilt University Medical Center, Department of Radiology and Radiological Sciences, Medical Center North 1161 21st Ave. S., Nashville, USA, 37232
[e]Vanderbilt University Medical Center, Department of Neurological Surgery, 1211 Medical Center Drive, Nashville, TN 37232, Nashville, USA, 37232
[f]Vanderbilt University Medical Center, Department of Otolaryngology – Head and Neck Surgery, 1211 Medical Center Drive, Nashville, TN 37232, Nashville, USA, 37232

Corresponding Author:
Winona Richey
1225 Stevenson Center Ln
Stevenson Center 5824
Nashville, TN 37240
winona.richey@vanderbilt.edu
ORCID: 0000-0001-9697-4069

Co-author ORCIDs:
Jon Heiselman: 0000-0002-4414-8846
Ma Luo: 0000-0002-2928-0996
Michael Miga: 0000-0002-0694-9765

ABSTRACT
Purpose. To reduce reoperation rates for image guided breast conserving surgery, the enhanced sensitivity of magnetic resonance (MR) supine imaging may be leveraged. However, accurate tissue correspondence between images and their physical counterpart in the surgical presentation is challenging due to breast deformations (e.g. from patient/arm position changes, and operating room table rotation differences). In this study, standard rigid registration methods are employed and tissue deformation is characterized.
Methods. On n=10 healthy breasts, surface displacements were measured by comparing intraoperative fiducial locations as the arm was moved from conventional MR scanning positions (arm-down and arm-up) to the laterally extended surgical configuration. Supine MR images in the arm-down and arm-up positions were registered to mock intraoperative presentations.
Results. Breast displacements from a supine MR imaging configuration to a mock surgical presentation were 28.9 ± 9.2 mm with shifts occurring primarily in the inferior/superior direction. With respect to supine MR-to-surgical alignment, the average fiducial, target, and maximum target registration errors were 9.0 ± 1.7 mm, 9.3 ± 1.7 mm, and 20.0 ± 7.6 mm, respectively. Even when maintaining similar arm positions in the MR image and mock surgery, the respective averages were 6.0 ± 1.0 mm, 6.5 ± 1.1 mm and 12.5 ± 2.8 mm.
Conclusion. From supine MR positioning to surgical presentation, the breast undergoes large displacements (9.9–70.1 mm). The data also suggest that significant nonrigid deformations (9.3 ± 1.7 mm with 20.0 mm average maximum) exist that need to be considered in image guidance and modeling applications.

Keywords: breast conserving surgery, image guided surgery, lumpectomy, supine MR, registration, computational modeling.

1 Introduction

High reoperation rates in breast conserving surgery have been referred to as "the other breast cancer epidemic," [1] and have been reported as 10–29% in recent years [2-4]. Newly adopted localization strategies are largely based on preoperative placement of invasive markers [5-10]. However, with these approaches it can be difficult to understand lesion position and extent, particularly at depth. An alternative approach is to leverage medical imaging data in real-time to guide surgery. For example, ultrasound image guidance has been shown to outperform seed-based methods with positive margin rates ranging from 0–14% [11-16]. Unfortunately, only 50% of non-palpable tumors are visible on ultrasound [17].

An image guidance platform that could integrate magnetic resonance (MR) imaging would provide more comprehensive guidance for the majority of patients. Such a system would provide detailed subsurface anatomy, higher sensitivity [18], and enhanced lesion location and extent with methods like dynamic contrast enhanced MR [19], particularly for ultrasound-occult cancer. The use of MR data to enhance localization in real time is limited by differences between the diagnostic

(prone) and surgical theater (supine) presentations. From prone to supine imaging, breast tissue shifts range 10–85 mm [20-22]. Additional confounding factors include differences in tumor volume, surface area, sphericity, and distances from the only available landmarks (the chest wall, skin, and nipple) [20-22].

Several surgical guidance frameworks have been introduced to register, or align, breast MR data to the surgical presentation (primarily prone to supine registration [23,24]). Recent advances have led groups to pursue supine MR [25-28] due to comparable imaging sensitivity and better initial alignment to surgical presentation. Barth *et al.* [29] expanded on the system of Pallone *et al.* [27,28] creating a custom supine MR image guidance system for breast conserving surgery relying on rigid registration, and achieving 9% positive margin rates, compared with 19% by wire guidance. In a similar work, Conley *et al.* developed a custom image-to-physical nonrigid registration method and demonstrated tumor centroid localization errors of 5.3 and 5.5 mm, outperforming rigid alignment error of 6.5 and 12.5 mm respectively [30,31]. Ebrahimi *et al.* implemented a thin-plate spline registration to predict tumor motion due to abduction of the arm [32]. While supine MR offers improved alignment, the above works suggest there are still uncharacterized discrepancies in tissue location between imaging and surgery presentations (e.g. effects from patient position, arm position, and surgical table rotation). This paper reports the nature of breast deformation from supine imaging-to-surgical presentation and evaluates the accuracy of rigid registration in the context of a supine MR image-guided approach.

2 Methods

2.1 Intraoperative Surgical Monitoring Platform

A custom data collection system [33] (**Fig. 1a)** was developed with stereo cameras (FLIR, Richmond, BC, Canada) for breast surface acquisition, optically tracked instruments (Northern Digital Inc., Waterloo, ON, Canada), intraoperative ultrasound (BK Medical, Peabody, MA, USA), and a guidance module implemented in 3D Slicer [34]. The module registers all patient data to MR image space, and presents the surgeon with the position of their tracked tool in relation to all other aspects of the scene including the breast model, lesion model, fiducial positions, and tracked ultrasound images. The system in **Fig 1a** is in use with a tracked stylus.

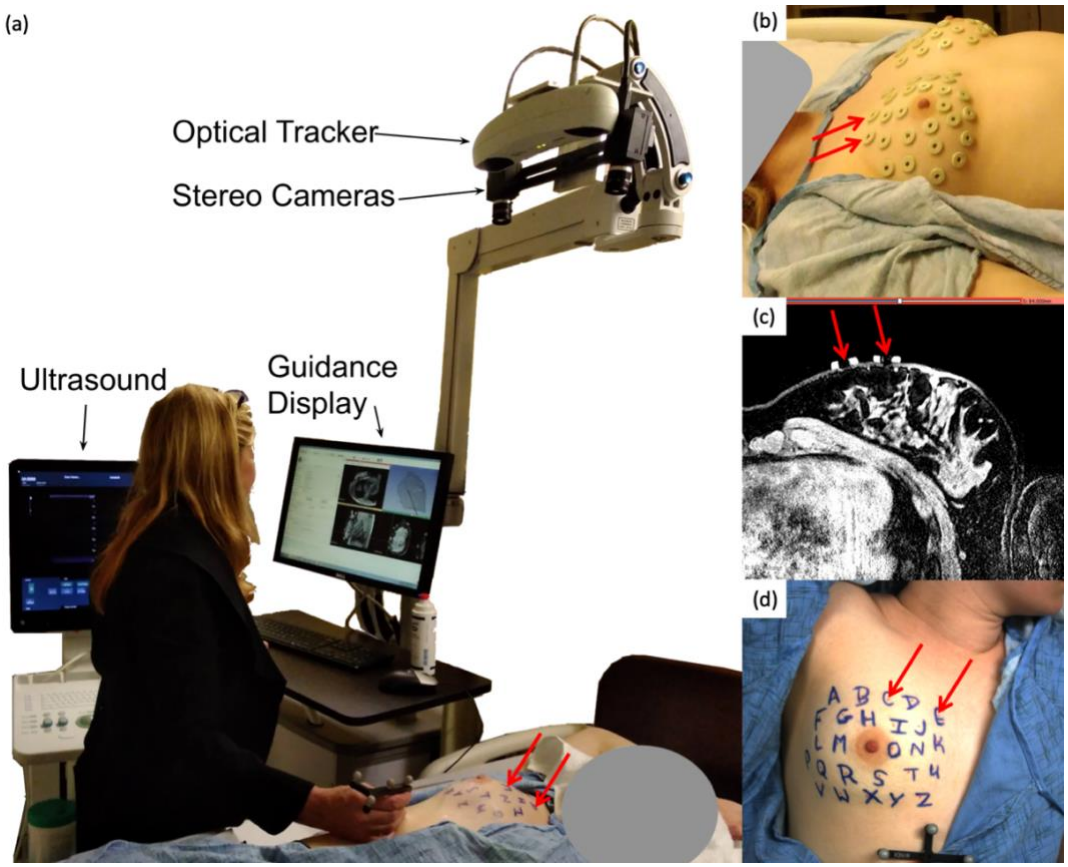

Fig. 1 Data collection system and fiducial distribution. Red arrows indicate fiducial locations. (a) Data collection in the arm-up position with the rigidly coupled instrument tracker and stereo camera pair, ultrasound machine, and guidance display. (b) Twenty six MR visible fiducials distributed across each breast. (c) Two fiducials visible on an axial slice of a supine MR image. (d) Anterior view from one RGB camera in the mock intraoperative setting; the center of each MR fiducial marked with red ink, and labeled with a blue hand drawn letter.

2.2 Human Data Collection

Experimental protocols were approved by the Vanderbilt University Institutional Review Board and six healthy volunteers were enrolled with informed consent. Of the twelve breasts, two were excluded from analysis: one due to subject movement during data collection, and one due to incomplete data. Volunteers ranged in age from 23–57 (average 30 ± 13) years. Breast volumes, as manually segmented from an arm-down supine MR, ranged from 459–1230 cm^3 (mean: 681 ± 214 cm^3). With each case, 26 adhesive synthetic MR-visible fiducial markers (IZI Medical Products, Owing Mills, MD) were placed on the skin with approximately equal sampling across the breast surface (**Fig. 1b**). The number of fiducials was chosen to sufficiently sample the surface based on three previous works [35,36,32]. To adequately and densely cover the surface of the breast, while providing precise point-to-point correspondence, 26 fiducial points were used. All measurements successfully identified at least 23 fiducials, and 82% contained all 26 fiducials.

MR data were collected in conventional closed bore 3T MR scanners (Philips Healthcare, Best, The Netherlands) using a T1-weighted, 3D turbo field echo sequence with fat suppression. One volunteer was imaged with an Ingenia Elition D-Stream wide bore, and the remaining five volunteers were imaged with an Ingenia D-Stream. A 16-channel torso coil was laid over the chest and supported with padding placed on the sternum to reduce breast compression. Multiple available clinical scanners were used across subjects with one of two voxel resolutions, $0.357\times0.357\times1mm^3$, or $0.391\times0.391\times1mm^3$ voxel size. To effectively capture the full range of breast motion between two arm position extremes, MR data were collected in two positions: with the ipsilateral arm down by the torso and then up by the head. The contralateral arm was down for both scans. Full lateral extension was not possible due to bore constraints. In both MR images,

locations of the MR-visible fiducials (**Fig. 1c**) were manually localized, and labeled in 3D Slicer with an English alphabet character-based label (A–Z). Fiducial labels provide intuitive correspondence between the model and physical space.

Less than 24 hours after MR imaging, the subject was moved to a mock surgical presentation area for additional data collection. The center of each fiducial was marked as a distinct ink dot, then the MR-visible fiducials were removed. Once removed, a letter label was then specifically inked onto the skin surrounding each inked fiducial dot (**Fig. 1d**). This process allowed the fiducial center to be identified on the subject using manual digitization via an optically tracked wand (stylus) as well as determined (potentially automatically) with the stereo cameras using optical character detection. In surgery, patients are typically oriented in an oblique supine position, with the operating table tilted slightly such that the ipsilateral arm is raised. This rotation of the table brings the breast to a more favorable position for lesion excision. To simulate this rotation, in our mock surgical presentation, padding was placed underneath the ipsilateral shoulder and upper torso. Data were then collected in three positions: with the ipsilateral arm down, abducted to 90 degrees from the torso (T-shape, the typical surgical presentation), and up by the head. Fiducial locations in the mock surgical setting were collected with a handheld optically tracked stylus. To allow quadrantized analysis, each fiducial location was manually assigned to one of the four conventional anatomical breast quadrants (upper outer, upper inner, lower outer, lower inner). Fiducials were assigned to quadrants by assessing fiducial locations in 3D space relative to the nipple and referencing RGB stereo camera images.

2.3 Breast Shift Among Range of Arm Positions

Breast surface displacements were measured by comparing intraoperative fiducial locations as the arm was moved in a mock surgical setting. Euclidean distances between

corresponding points were computed for 3 shifts: (i) arm-down to T-shape, (ii) T-shape to arm-up, and (iii) arm-down to arm-up. The first measured shift represents the typical arm motion from preoperative supine MR imaging to surgical position. The second measured shift was performed to capture an alternative preoperative supine MR position with the arm-up. The third breast shift represents the effect of the full range of arm motion. The magnitude and direction of displacement were measured for each shift, and compared between shifts. The directionality of displacement was analyzed by comparing the three orthogonal components of displacement in the MR image space: medial/lateral, anterior/posterior, and superior/inferior. The directionality is reported in each anatomical direction as the percentage of the total displacement. Additionally, for each case the average displacement was computed in each quadrant. Displacements were compared among the four breast quadrants.

2.4 Image-to-Physical Registration Associated with Conventional Image-Guided Surgery Approaches

While Section 2.3 measured breast shift magnitude, it is important to distinguish rigid translations and rotations from nonrigid deformations. To study this, spatial discrepancies in breast fiducials were investigated after registering the fiducials between conventional supine MR imaging and mock surgical presentation. Using traditional point-based registration techniques, fiducial locations in MR image space were aligned with their corresponding positions that were optically digitized in the physical mock surgical setting. The rigid registration method is described in [37] and is an accepted standard in the field. Traditional metrics of fiducial registration error (FRE) and target registration error (TRE) are reported [37]. Briefly, the fiducial registration error (FRE) measures the general misalignment of fiducials as $FRE = \sqrt{\frac{1}{N}\sum_{i=1}^{N}|T(x_i) - y_i|}$ where N is the

number of corresponding fiducial points, $T(x_i)$ represents the rigidly transformed i^{th} fiducial point x_i into the same space as corresponding point y_i. The target registration error (TRE) represents an equivalent calculation but the point being compared in the two spaces is a novel point that was not used in determination of the rigid registration transformation, $T(*)$. Here, TRE was determined using a leave-one-out strategy where the transformation $T(*)$ is determined using N-1 fiducials. The N^{th} fiducial is treated as a novel target. This process is repeated iteratively treating each fiducial as a target to evaluate accuracy. TRE is established as the root mean square error over the entire cohort.

Registration error metrics are reported for each of the four image-to-physical registrations involving the mock operating room (OR) and conventional MR settings: (1) arm-down mock OR to arm-down MR (2) arm-up mock OR to arm-up MR, (3) T-shape mock OR (surgical position) to arm-down MR, and (4) T-shape mock OR to arm-up MR. For registration (3) – a likely surgical protocol, TRE is further evaluated by varying the number and distribution of fiducials to establish potential lower bounds required for good registration fidelity. These additional analyses focus particularly on the impact of fiducial distribution across the four breast quadrants. Beginning with a lower limit of using only *n=4* fiducials and proceeding to an upper limit of *n=23* fiducials, registrations were performed for each possible combination of *n* fiducials. Any fiducials not used in the registration were treated as novel targets for the determination of TRE. Here, since all cases have at least 24 corresponding fiducials recognized for registration (3), the upper limit of *n=23* is used to ensure that registration accuracy may be computed on at least one target for each case. TRE was averaged by case, and then across all cases. Some of these combinations represent unrealistic and unbalanced fiducial distributions. Therefore, an alternative combinatorial approach was also used to evaluate the impact of systematically distributing fiducials across quadrants. The

process begins by requesting one fiducial from each quadrant to be used in registration, then incrementing. This quadrantized approach includes all combinations where the differences among the number of fiducials requested from each quadrant are no more than one. When the number of fiducials from a quadrant requested for registration exceeds the number of fiducials in the quadrant, all fiducials in that quadrant are drawn and additional combinations are included reserving one fiducial in that quadrant as a target. All combinations are ensured to be unique.

2.5 Statistical Tests

For each metric reported, the distribution of samples was tested for normality using a one-sample Kolmogorov-Smirnov test. Each distribution was found to be approximately normally distributed. A paired-t test ($\alpha = .05$) was used to test significance and power, given the sample size of 10 breasts. Magnitude and direction of displacement were compared with paired *t*-tests ($p<0.05$). Displacements were compared among the four breast quadrants with a paired *t*-test ($p<0.008$ with Bonferroni correction). Tests with power greater than 80% are considered strongly powered.

3 Results

3.1 Breast Shift Among Range of Arm Positions

With the subject otherwise stationary in the mock OR setting, the average displacement, i.e. shift, from the arm-down to T-shape position was 28.9 ± 9.2 mm (range: 9.9–70.1 mm), while the average displacement from the arm-up to T-shape position was 27.6 ± 8.9 mm. This difference was not statistically significant ($p>.05$). The average displacement from the arm-down to arm-up position was 42.0 ± 15.4 mm, which was significantly greater ($p<0.05$) than the shift from arm-down to T-shape (power = 0.79) and the shift from arm-up to T-shape (power = 0.99). For

reference, each volunteer is assigned a lowercase letter and subjects are presented in the order of decreasing breast volume (*a*–*f*). Subjects are consistently labeled with this convention across all figures and tables. Results are reported in **Table 1**.

Table 1 Surface fiducial displacements in the supine position and registration error metrics for image-to-physical registrations reported in millimeters (mm).

Case		Breast Volume (cm^3)	Displacement (mm) Mean ± Std		
			Arm-down to T-shape	Arm-up to T-shape	Arm-down to Arm-up
a	L	1,230	26.8 ± 5.2	39.4 ± 13.1	58.0 ± 14.8
b	R	730	39.5 ± 10.1	29.1 ± 8.9	55.8 ± 17.9
	L	694	33.5 ± 10.0	24.3 ± 9.4	54.7 ± 16.6
c	R	693	40.5 ± 6.4	26.3 ± 6.1	38.5 ± 11.4
	L	668	38.5 ± 6.2	22.9 ± 2.9	36.9 ± 8.2
d	R	688	14.5 ± 2.6	19.7 ± 5.1	21.9 ± 5.4
	L	581	17.4 ± 1.9	13.2 ± 5.2	18.2 ± 3.9
e	R	595	21.3 ± 3.5	30.4 ± 7.3	42.4 ± 8.6
	L	474	29.0 ± 5.0	43.9 ± 10.5	62.1 ± 14.8
f	L	459	28.4 ± 3.5	26.7 ± 6.7	31.6 ± 8.7
Mean: 681cm³			*28.9 ± 9.2*	*27.6 ± 8.9*	*42.0 ± 15.4*

For the left breast of each volunteer, displacement magnitude and direction are displayed on the breast model segmented from the MR image (**Fig. 2)**. Fiducial displacements, shown with arrows, were interpolated across the model surface using natural neighbor interpolation, as implemented in MATLAB, to produce the colored meshes. For each mesh, the sternum is on the left with the armpit towards the top right, as shown by the human outline in the bottom right of Fig. 2.

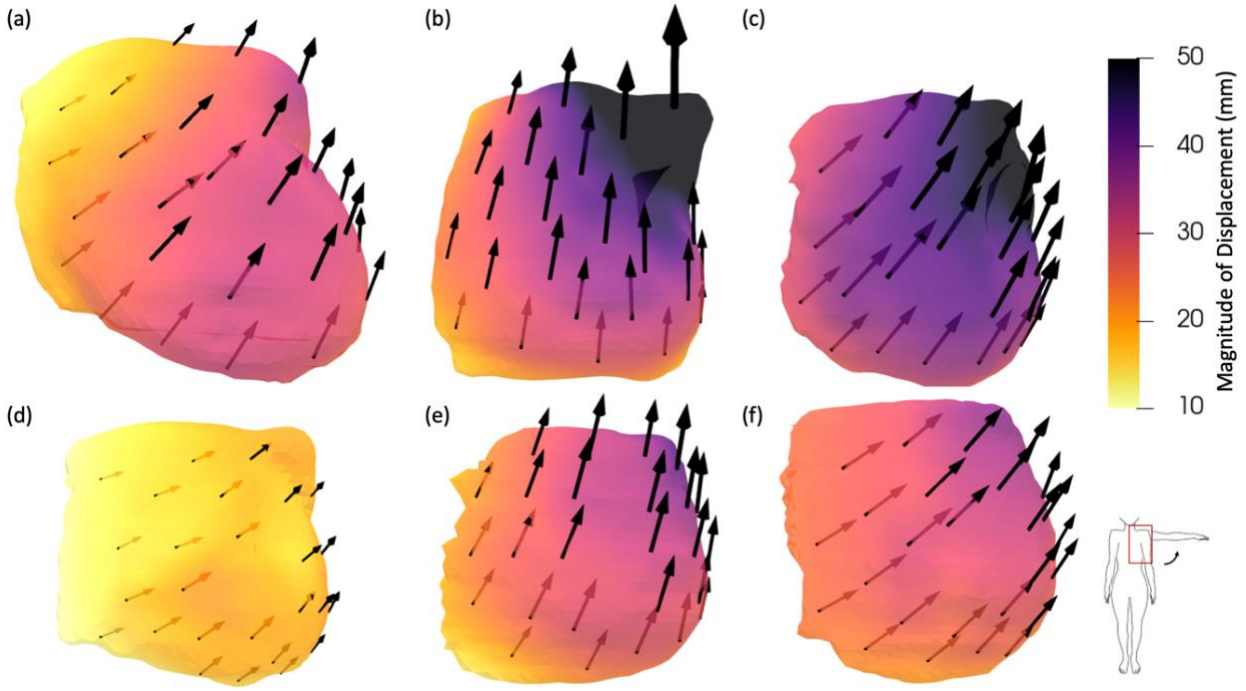

Fig. 2 Breast surface displacements associated with arm movement from the arm-down position to intraoperative position. Arrow vectors placed at fiducial locations show the direction of displacement and are scaled according to the magnitude of displacement.

The percentage of displacement in each of the three orthogonal directions (medial/lateral, anterior/posterior, superior/inferior) is shown in **Fig. 3**. The percentage of displacement in the medial/lateral direction was statistically larger in the arm-up to T-shape shift when compared to the two other shifts (power = 0.66 when compared to arm-down to T-shape shift and power = 0.98 when compared to arm-down to arm-up shift). The percentage of displacement in the superior/inferior direction was significantly larger in the arm-down to arm-up position change when compared to the two other positional changes (power = 0.87 when compared to arm-down to T-shape shift and power = 0.99 when compared to arm-up to T-shape shift). In the anterior/posterior direction, the percentage of displacement was significantly larger for the arm-down to T-shape shift only when compared to the arm-down to arm-up shift (power = 0.91).

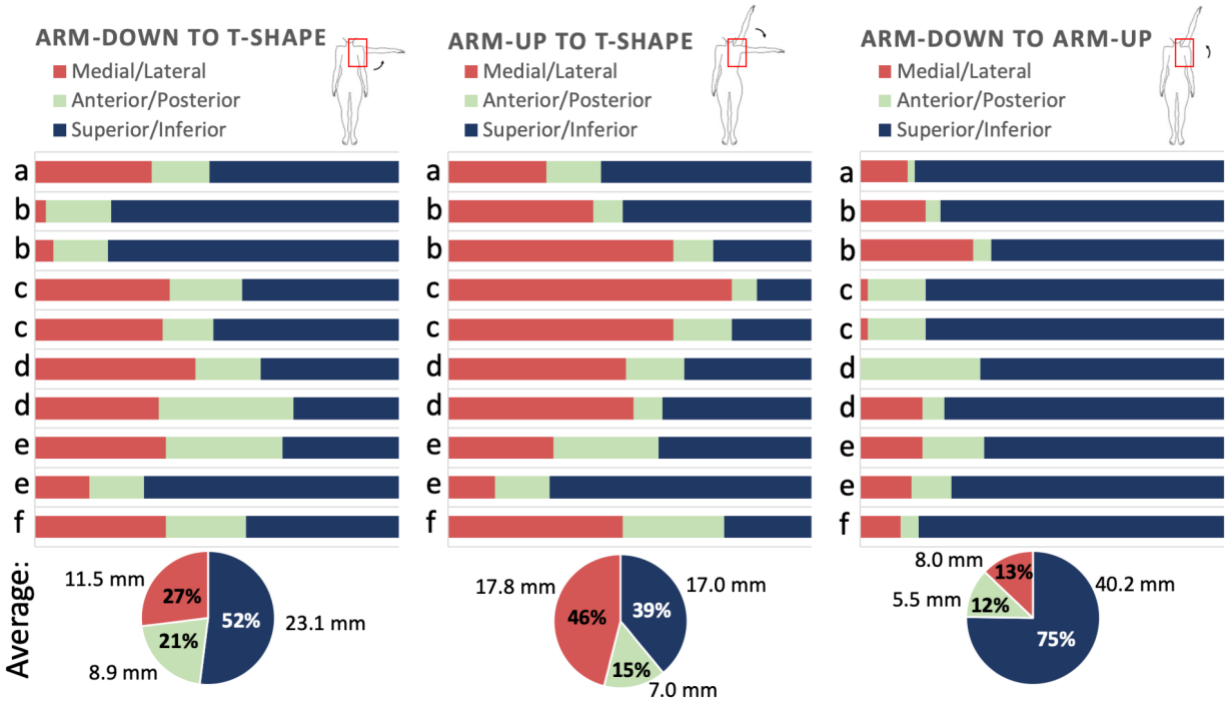

Fig. 3 Directionality of breast surface displacements associated with arm movement in the supine position with arm motion illustrated for each of the three positional changes. Average percentage and magnitude of displacement in each direction is displayed at the bottom.

3.1.1 Analysis of Breast Shift by Anatomical Quadrant

Average displacement differed among the four conventional anatomical quadrants, illustrated in **Fig 4a**. For the arm-down to T-shape pose change, average displacements in the upper outer quadrant were significantly larger than averages in all other quadrants (power > 0.98) as shown in **Fig 4b**. From T-shape to the arm-up position, the upper outer quadrant shifted significantly more and the lower inner quadrant shifted significantly less than all other quadrants (power > 0.99). When comparing average quadrant displacements from the arm-down to arm-up positions, all comparisons were significantly different (power > 0.90) as shown in **Fig. 4c**. The line of equivalence is plotted as a reference, showing where the displacement associated with quadrant A on the *y*-axis is equivalent to the displacement of the comparator quadrant B on the *x*-axis. Deviations from this line of equivalence are readily visualized in **Fig. 4**.

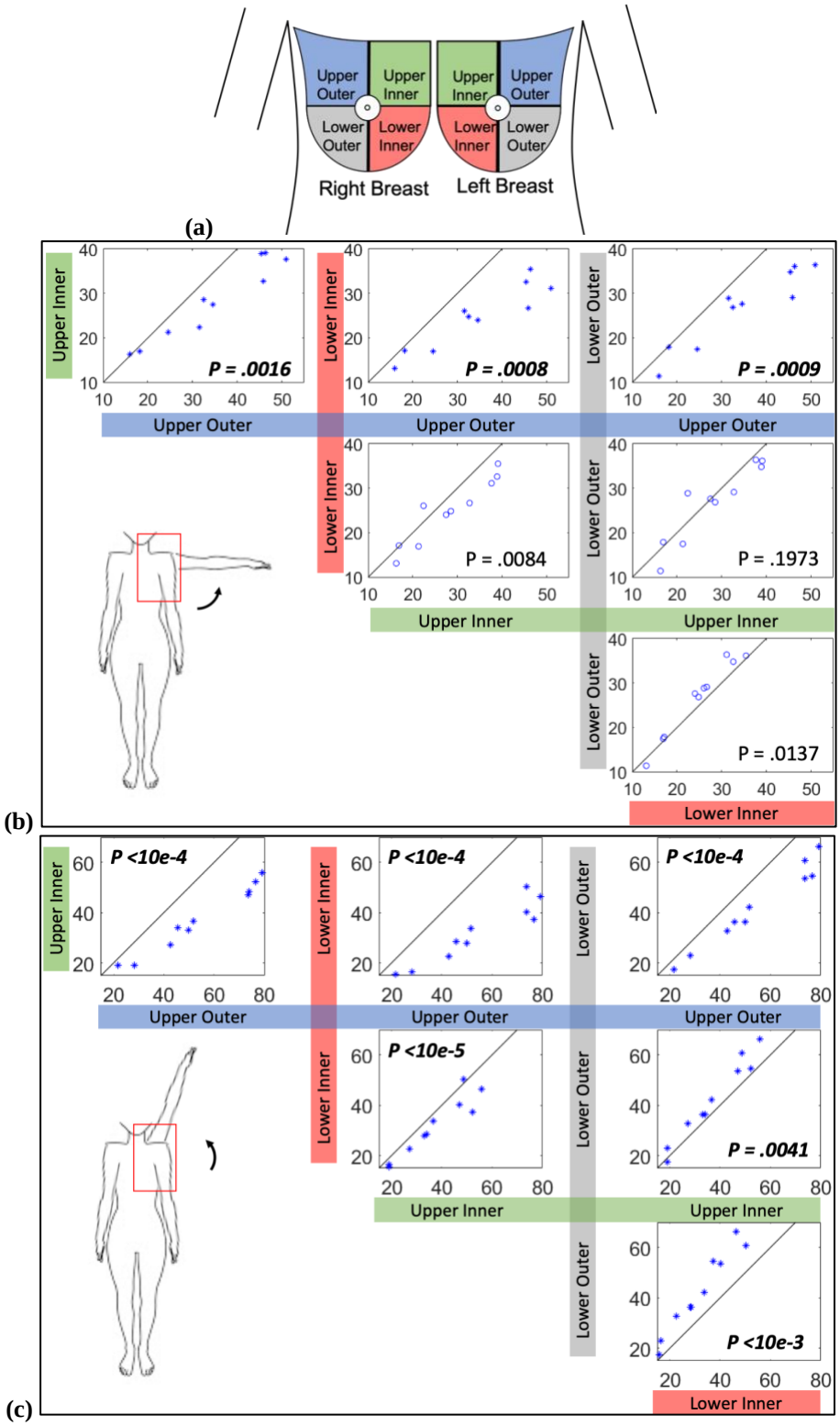

Fig. 4 Comparison of average displacements for each pair of quadrants. Each plot point represents the average displacement in two quadrants for one case. Significantly different shifts are plotted as asterisks (*), and *p*-values are reported. The line *y=x*, where quadrant displacements are equivalent, is shown in black. (a) Color coded quadrants of the breast (b) Comparison of average quadrant displacements from arm-down to T-shape (c) comparison of average quadrant displacements from arm-down to arm-up.

3.2 Image-to-Physical Registration Results Associated with Conventional Image-Guided Surgery Approaches

Registration error metrics are reported (**Table 2**) for each combination of preoperative and intraoperative data: (1) arm-down mock OR to arm-down MR (2) arm-up mock OR to arm-up MR, (3) T-shape mock OR (surgical position) to arm-up MR, and (4) T-shape mock OR to arm-down MR. The first two registrations quantify breast deformations for equivalent arm poses; the third and fourth registrations quantify the deformation from the preoperative images to surgical positioning. Fiducial registration error (FRE) values were 5.8 ± 0.8 mm and 6.2 ± 1.2 mm for registrations (1) and (2) respectively. Target registration error (TRE) values were 6.3 ± 0.9 mm and 6.7 ± 1.3 mm for registrations (1) and (2) respectively. For registrations from image space to surgical presentation (T-shape), FRE was 7.9 ± 1.6 mm using the arm-up MR image (3), and 9.0 ± 1.7 mm using the arm-down MR image (4). TREs were 8.6 ± 1.8 mm and 9.3 ± 1.7 mm for registrations (3) and (4) respectively. On average for deformation (4), the maximum target error was 20.0 ± 7.6 mm. **Fig. 5** shows TRE at each fiducial location on a wireframe representation of the breast surface. Furthermore, image to physical registrations in the same arm pose were compared to registrations with differing arm poses (imaging to surgical position). More specifically, (1) was compared to (4) and similarly (2) was compared to (3). These registration errors were significantly different (power > 0.95), indicating significant nonrigid deformations are due to arm motion in the supine position.

In registrations for the arm-down to T-shape deformation, the most likely surgical protocol, average TRE decreased asymptotically with an increasing number of fiducials with a final limit of 8.5 mm. The quadrantized method approached the limit faster than the non-quadrantized method. For $n > 10$ fiducials the two approaches are not statistically different.

Table 2 Registration error metrics (in millimeters, mm) for image-to-physical registrations of surface points.

Case		Breast Volume (cm^3)	Registration Error (mm)											
			Arm-Down MR to Arm-Down Mock OR			Arm-Up MR to Arm-Up Mock OR			Arm-Up MR to Surgical Position			Arm-Down MR to Surgical Position		
			FRE	TRE	Max TRE	FRE	TRE	Max TRE	FRE	TRE	Max TRE	FRE	TRE	Max TRE
a	L	1,230	7.4	7.9	14.8	5.8	6.2	9.9	10.0	10.9	17.7	10.3	10.9	21.0
b	R	730	5.3	5.8	10.9	3.9	4.2	7.4	5.0	5.6	11.9	9.7	10.4	27.8
	L	694	6.3	6.9	13.9	5.5	6.2	11.8	8.2	9.2	16.3	11.3	12.1	36.4
c	R	693	4.9	5.3	10.0	5.7	6.2	12.0	8.0	8.8	13.2	9.4	10.1	23.3
	L	668	5.5	5.9	10.0	7.9	8.6	16.1	7.6	8.2	18.4	9.6	10.3	20.1
d	R	688	5.2	5.5	8.1	6.3	6.7	10.0	6.6	7.0	10.7	10.5	8.0	11.1
	L	581	5.3	5.7	14.4	7.5	8.1	17.4	9.1	9.9	19.3	6.0	6.5	14.4
e	R	595	6.4	6.8	15.3	7.6	8.3	14.3	10.4	11.3	19.8	7.2	7.7	13.9
	L	474	6.7	7.1	15.6	5.8	6.2	12.8	7.0	7.6	16.3	8.1	8.6	16.8
f	L	459	5.4	5.8	14.3	6.0	6.5	11.3	7.3	7.8	14.4	7.7	8.2	15.6
Mean: 681cm³			*5.8*	*6.3*	*12.7*	*6.2*	*6.7*	*12.3*	*7.9*	*8.6*	*15.8*	*9.0*	*9.3*	*20.0*

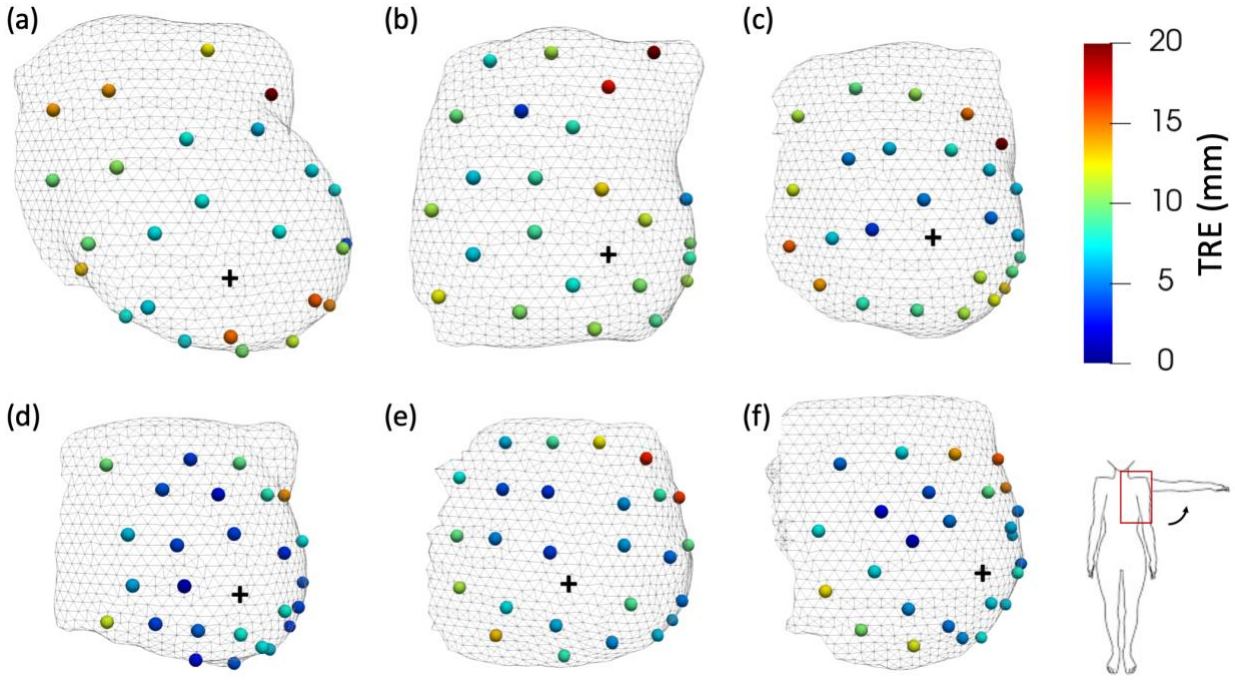

Fig. 5 Target registration error for arm-down supine MR to intraoperative position (T-shape mock OR) for the left breast of each subject. The nipple is marked by (+).

3.3 Impact of Instrumentation Error on Analysis

Registration error due to instrumentation was evaluated by rigidly aligning five sets of skin fiducial points collected with the subject in exactly the same position. Two main sources of error are possible: intrinsic instrumentation error associated with optical tracking and MR imaging

resolution, and localization error associated with an individual designating the location of a fiducial marker either using an optically tracked stylus on the patient or demarking the fiducial marker in a corresponding MR imaging set. While the error associated with intrinsic instrumentation error is documented by device characteristics [38], the impact of localization error needs to be assessed in practical use. To evaluate accuracy of fiducial localization on a subject in the T-shape surgical presentation position, the same fiducial locations were collected repeatedly for a total of five point sets. All combinations of point sets (5 choose 2) were registered, and the average FRE was determined to be 1.5 ± 0.1 mm. Similarly, the locations of the fiducials were designated in an MR image with the subject arm down and all combinations of point sets (5 choose 2) were registered providing a counterpart average FRE of 1.6 ± 0.4 mm.

For each measurement approach, an approximation standard of the upper limit of instrumentation error was defined as one standard deviation greater than the mean. This results in 1.6 mm and 2.0 mm for optical-stylus digitized and MR points respectively. In a worst-case scenario, these errors would sum to represent a combined instrumentation error, i.e. approximately 3.6 mm. When considering the remaining error after registering the supine MR images and surgical T-shape presentation, errors that are significantly greater than this 3.6 mm instrumentation error (paired t-test, $p<.05$) are assumed to be associated with deformations, i.e. nonrigid shape change. All registrations produced significantly greater errors; therefore, nonrigid components of deformation are significant and cannot be completely compensated for using a rigid registration approach. This analysis shows that nonrigid deformation between imaging and surgery is significant even for registrations between the same pose (i.e. (1) and (2)).

4 Discussion

At a fundamental level, the components of rigid and nonrigid deformation are considerable between MR-supine and OR-supine configurations. Across subjects, displacement and registration error varied in magnitude (9.0 mm average FRE with average maximum TRE of 20.0 mm) and spatial distribution suggesting that patient-specificity and real-time monitoring are likely needed within a resection guidance approach. Displacements were also largest in the upper outer quadrant, where disproportionately 38–54% of breast cancers occur [39-41]. This uneven shift among quadrants would also likely make rigid-registration based image guidance approaches particularly prone to error. Even with a high number of well-distributed fiducials, when registering conventional supine breast MR to surgical presentation each subject had a region with TRE above 10 mm, and many had regions with TRE above 20 mm. Comparing image-to-physical registration errors in the same vs. differing arm poses demonstrated that there are significant nonrigid deformations due to arm motion. Going further, even when the arm poses were kept consistent between MR and mock surgery positions, nonrigid error was still present (average errors of 6.5 mm with average maximum TRE of 12.5 mm) and significantly greater than instrumentation error. This suggests that even under ideal conditions, nonrigid deformation is likely an important factor to consider. Other important considerations are number of fiducials and preferred MR position. For rigid registration, greater than 10 fiducials and distribution across all four quadrants is recommended. Neither arm-up nor arm-down supine MR position is preferred when considering displacement magnitude or registration error. However, the significant difference in directionality could impact the difficulty of modeling these deformations.

To the best of our knowledge, this work is the first to report such a comprehensive characterization of image-to-surgical deformations. While limited to the breast surface,

displacements and registration errors are reported for densely sampled corresponding points. In a related work, Ebrahimi *et al* measured tumor displacement from the arm-down position, to an arm up position in supine MR images. The center of mass displacements for six tumors were reported between 10.9 and 46.8 millimeters from full abduction of the arm. Rigid registration errors (TRE) for tumors' centers of mass were between 2.6 and 17.9 mm. The magnitudes of these subsurface measurements are remarkably comparable and consistent with our measurements provided here thus proving a similar scale and range for both displacement and registration error.

There are several limitations to this work. The sample size is small and not representative of breast cancer patient demographics. Breast cancer patients are typically older than the average age of the reported cohort, with most patients in the age range of 50–70 years old [42] and subject to differing breast consistency. Further study remains to conclusively evaluate the effects of numerous anatomical factors on breast displacement and registration error (e.g. volume, density, and placement/distribution of breast tissue). The position of the breast on the torso was an unexpected confounding factor in this dataset. Larger, and particularly more laterally set breasts are deformed by contact with the arm in the arm down position. Similarly, these breasts could also experience larger forces during arm motion due to spatial relationships to ligaments and axillary skin. Breast shape and the position of breast tissue on the rib cage likely impact deformation and registration error as well, but these effects have not been investigated in this work. Expanding this data set is a next step to establish trends regarding the impact of breast volume on displacement or registration error.

Another limitation of the work is associated with workflow. In practice, some seed-based targets can be implanted up to 30 days before surgery [6,43] allowing workflow and cost benefits by enabling scheduling flexibility [44]. Comparatively, fiducial placement likely reduces patient

discomfort but with more restrictive scheduling. In the framework discussed herein, there would also be modifications to necessary imaging. Supine MR is not standard of surgical care and would likely increase imaging costs. However, workflow modifications must also be considered within the context of current reoperation rates. A single-pass negative-margin breast conserving surgery procedure would have great potential patient and cost benefits. Lastly, this work has been limited to breast surface analysis. Integration of tracked intraoperative ultrasound, as in **Fig 1**, allows subsurface features to be incorporated (i.e. tumor margins, implanted biopsy clips, etc.). While rigid registration often relies on surface fiducials, the addition of subsurface ultrasound data could help to constrain a nonrigid modeling approach. **Fig. 6** shows an example under development and awaits further study.

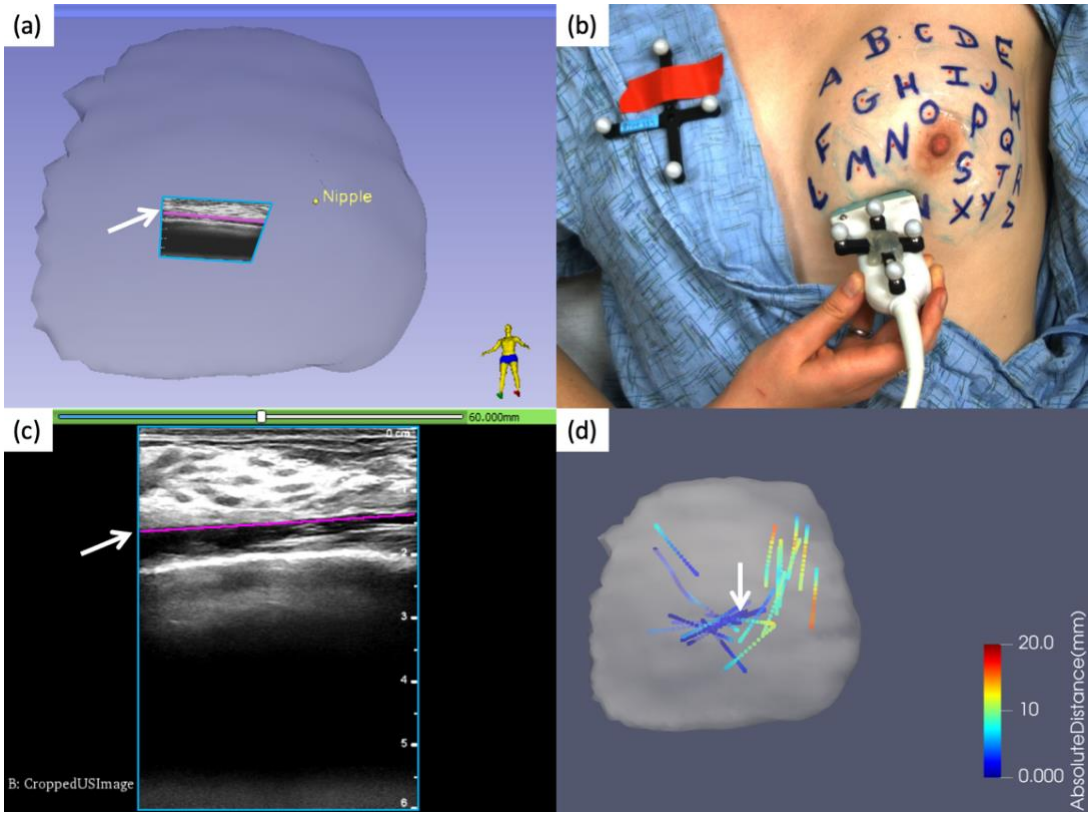

Fig. 6 Ultrasound data in an image guidance system, with a white arrow indicating this chest wall segmentation: (a) breast model as segmented from the MR image with tracked ultrasound plane in blue, and the chest wall segmented in magenta; (b) ultrasound image acquisition in the mock OR; (c) ultrasound image outlined in blue with the segmented chest wall surface in magenta; (d) acquired chest wall contour data on the breast model where color indicates the closest point residual with its MR counterpart after rigid registration.

5 Conclusion

While work is ongoing with supine MR and rigid registration guidance [29,26,30], results here have demonstrated that for supine MR-to-OR alignment strategies, nonrigid deformations are present and significant. Navigation systems will need to improve accuracy to compete with, and improve beyond, implanted marker-based guidance. Future strategies that use sparse readily-available localization and imaging data coupled to nonrigid registration approaches could potentially offer the next cost-effective revolution in improved surgical accuracy.

Declarations

Funding: This work was supported by NIH-NIBIB awards T32EB021937, R21EB022380, R01EB027498, and Vanderbilt grant 1S10OD021771-01.

Conflicts of Interest/Competing Interests: The authors have no conflicts of interest to disclose.

Ethics approval: All procedures performed in studies involving human participants were in accordance with the ethical standards of the institutional and/or national research committee and with the 1964 Helsinki declaration and its later amendments or comparable ethical standards.

Consent to participate: All data was collected with Vanderbilt University Institutional Review Board approval. Freely-given, informed consent to participate in the study was obtained from all participants.

Consent to publication: The authors affirm that human research participants provided informed consent for publication of the images.

References

1. Cody HS, 3rd, Van Zee KJ (2015) Reexcision--The Other Breast Cancer Epidemic. N Engl J Med 373 (6):568-569. doi:10.1056/NEJMe1507190

2. Gladden AAH, Sams S, Gleisner A, Finlayson C, Kounalakis N, Hosokawa P, Brown R, Chong T, Mathes D, Murphy C (2017) Re-excision rates after breast conserving surgery following the 2014 SSO-ASTRO guidelines. Am J Surg 214 (6):1104-1109
3. van Leeuwen MT, Falster MO, Vajdic CM, Crowe PJ, Lujic S, Klaes E, Jorm L, Sedrakyan A (2018) Reoperation after breast-conserving surgery for cancer in Australia: statewide cohort study of linked hospital data. BMJ open 8 (4):e020858
4. Hughes L, Hamm J, McGahan C, Baliski C (2016) Surgeon volume, patient age, and tumor-related factors influence the need for re-excision after breast-conserving surgery. Ann Surg Oncol 23 (5):656-664
5. Schermers B, van der Hage JA, Loo C, Peeters MV, Winter-Warnars H, van Duijnhoven F, Ten Haken B, Muller S, Ruers T (2017) Feasibility of magnetic marker localisation for non-palpable breast cancer. Breast 33:50-56
6. Lamb LR, Bahl M, Lehman CD (2018) Evaluation of a nonradioactive magnetic marker wireless localization program. AJR Am J Roentgenol 211 (4):W202-W202
7. Langhans L, Tvedskov TF, Klausen TL, Jensen MB, Talman ML, Vejborg I, Benian C, Roslind A, Hermansen J, Oturai PS, Bentzon N, Kroman N (2017) Radioactive Seed Localization or Wire-guided Localization of Nonpalpable Invasive and In Situ Breast Cancer A Randomized, Multicenter, Open-label Trial. Ann Surg 266 (1):29-35. doi:10.1097/sla.0000000000002101
8. Velazco CS, Wasif N, Pockaj BA, Gray RJ (2017) Radioactive seed localization for breast conservation surgery: Low positive margin rate with no learning curve. Am J Surg 214 (6):1091-1093
9. Cox CE, Garcia-Henriquez N, Glancy MJ, Whitworth P, Cox JM, Themar-Geck M, Prati R, Jung M, Russell S, Appleton K, King J, Shivers SC (2016) Pilot Study of a New Nonradioactive Surgical Guidance Technology for Locating Nonpalpable Breast Lesions. Ann Surg Oncol 23 (6):1824-1830. doi:10.1245/s10434-015-5079-x
10. Mango VL, Wynn RT, Feldman S, Friedlander L, Desperito E, Patel SN, Gomberawalla A, Ha R (2017) Beyond wires and seeds: reflector-guided breast lesion localization and excision. Radiology 284 (2):365-371
11. Volders JH, Haloua MH, Krekel NMA, Negenborn VL, Kolk RHE, Cardozo A, Bosch AM, de Widt-Levert LM, van der Veen H, Rijna H, van Amerongen A, Jozwiak K, Meijer S, van den Tol MP (2017) Intraoperative ultrasound guidance in breast-conserving surgery shows superiority in oncological outcome, long-term cosmetic and patient-reported outcomes: Final outcomes of a randomized controlled trial (COBALT). Eur J Surg Oncol 43 (4):649-657. doi:10.1016/j.ejso.2016.11.004
12. Eggemann H, Ignatov T, Costa SD, Ignatov A (2014) Accuracy of ultrasound-guided breast-conserving surgery in the determination of adequate surgical margins. Breast Cancer Res Treat 145 (1):129-136
13. Rubio IT, Esgueva-Colmenarejo A, Espinosa-Bravo M, Salazar JP, Miranda I, Peg V (2016) Intraoperative Ultrasound-Guided Lumpectomy Versus Mammographic Wire Localization for Breast Cancer Patients After Neoadjuvant Treatment. Ann Surg Oncol 23 (1):38-43. doi:10.1245/s10434-015-4935-z
14. Karanlik H, Ozgur I, Sahin D, Fayda M, Onder S, Yavuz E (2015) Intraoperative ultrasound reduces the need for re-excision in breast-conserving surgery. World J Surg Oncol 13 (1):321
15. Cakmak GK, Emre AU, Bahadir B, Tascilar O, Ozkan S (2017) Surgeon performed continuous intraoperative ultrasound guidance decreases re-excisions and mastectomy rates in breast cancer. Breast 33:23-28. doi:10.1016/j.breast.2017.02.014

16. Barentsz MW, van Dalen T, Gobardhan PD, Bongers V, Perre CI, Pijnappel RM, van den Bosch M, Verkooijen HM (2012) Intraoperative ultrasound guidance for excision of non-palpable invasive breast cancer: a hospital-based series and an overview of the literature. Breast Cancer Res Treat 135 (1):209-219. doi:10.1007/s10549-012-2165-7
17. Klimberg VS (2003) Advances in the diagnosis and excision of breast cancer. Am Surg 69 (1):11
18. Mann RM, Kuhl CK, Moy L (2019) Contrast-enhanced MRI for breast cancer screening. J Magn Reson Imaging 50 (2):377-390
19. Byrd BK, Krishnaswamy V, Gui J, Rooney T, Zuurbier R, Rosenkranz K, Paulsen K, Barth RJ (2020) The shape of breast cancer. Breast Cancer Res Treat:1-8
20. Gombos EC, Jayender J, Richman DM, Caragacianu DL, Mallory MA, Jolesz FA, Golshan M (2016) Intraoperative supine breast MR imaging to quantify tumor deformation and detection of residual breast cancer: preliminary results. Radiology 281 (3):720-729
21. Mallory MA, Sagara Y, Aydogan F, DeSantis S, Jayender J, Caragacianu D, Gombos E, Vosburgh KG, Jolesz FA, Golshan M (2017) Feasibility of Intraoperative Breast MRI and the Role of Prone Versus Supine Positioning in Surgical Planning for Breast-Conserving Surgery. Breast J 23 (6):713-717. doi:10.1111/tbj.12796
22. Satake H, Ishigaki S, Kitano M, Naganawa S (2016) Prediction of prone-to-supine tumor displacement in the breast using patient position change: investigation with prone MRI and supine CT. Breast Cancer 23 (1):149-158
23. Carter T, Tanner C, Beechey-Newman N, Barratt D, Hawkes D MR navigated breast surgery: method and initial clinical experience. In: International Conference on Medical Image Computing and Computer-Assisted Intervention, 2008. Springer, pp 356-363
24. Carter TJ, Tanner C, Crum WR, Beechey-Newman N, Hawkes DJ A framework for image-guided breast surgery. In: International Workshop on Medical Imaging and Virtual Reality, 2006. Springer, pp 203-210
25. Sakakibara M, Nagashima T, Sangai T, Nakamura R, Fujimoto H, Arai M, Kazama T, Hashimoto H, Nakatani Y, Miyazaki M (2008) Breast-Conserving Surgery Using Projection and Reproduction Techniques of Surgical-Position Breast MRI in Patients with Ductal Carcinoma In Situ of the Breast. J Am Coll Surg 207 (1):62-68. doi:https://doi.org/10.1016/j.jamcollsurg.2007.12.034
26. Alderliesten T, Loo C, Paape A, Muller S, Rutgers E, Peeters MJ, Gilhuijs K (2010) On the feasibility of MRI-guided navigation to demarcate breast cancer for breast-conserving surgery. Med Phys 37 (6):2617-2626. doi:10.1118/1.3429048
27. Pallone MJ, Poplack SP, Avutu HB, Paulsen KD, Barth RJ, Jr. (2014) Supine breast MRI and 3D optical scanning: a novel approach to improve tumor localization for breast conserving surgery. Ann Surg Oncol 21 (7):2203-2208. doi:10.1245/s10434-014-3598-5
28. Pallone MJ, Poplack SP, Barth Jr RJ, Paulsen KD Combining supine MRI and 3D optical scanning for improved surgical planning of breast conserving surgeries. In: Medical Imaging 2012: Image-Guided Procedures, Robotic Interventions, and Modeling, 2012. International Society for Optics and Photonics, p 83163B
29. Barth RJ, Krishnaswamy V, Paulsen KD, Rooney TB, Wells WA, Angeles CV, Zuurbier RA, Rosenkranz K, Poplack S, Tosteson TD (2019) A Randomized Prospective Trial of Supine MRI-Guided Versus Wire-Localized Lumpectomy for Breast Cancer. Ann Surg Oncol:1-10
30. Conley RH, Meszoely IM, Weis JA, Pheiffer TS, Arlinghaus LR, Yankeelov TE, Miga MI (2015) Realization of a biomechanical model-assisted image guidance system for breast cancer

surgery using supine MRI. Int J Comput Assist Radiol Surg 10 (12):1985-1996. doi:10.1007/s11548-015-1235-9
31. Conley RH, Meszoely IM, Pheiffer TS, Weis JA, Yankeelov TE, Miga MI Image to physical space registration of supine breast MRI for image guided breast surgery. In: Medical Imaging 2014: Image-Guided Procedures, Robotic Interventions, and Modeling, 2014. International Society for Optics and Photonics, p 90362N
32. Ebrahimi M, Siegler P, Modhafar A, Holloway CM, Plewes DB, Martel AL (2014) Using surface markers for MRI guided breast conserving surgery: a feasibility survey. Phys Med Biol 59 (7):1589-1605. doi:10.1088/0031-9155/59/7/1589
33. Richey WL, Heiselman J, Luo M, Meszoely IM, Miga MI Textual fiducial detection in breast conserving surgery for a near-real time image guidance system. In: Medical Imaging 2020: Image-Guided Procedures, Robotic Interventions, and Modeling, 2020. International Society for Optics and Photonics, p 113151L
34. Fedorov A, Beichel R, Kalpathy-Cramer J, Finet J, Fillion-Robin J-C, Pujol S, Bauer C, Jennings D, Fennessy F, Sonka M (2012) 3D Slicer as an image computing platform for the Quantitative Imaging Network. Magn Reson Imaging 30 (9):1323-1341
35. Heiselman JS, Miga MI The image-to-physical liver registration sparse data challenge: characterizing inverse biomechanical model resolution. In: Medical Imaging 2020: Image-Guided Procedures, Robotic Interventions, and Modeling, 2020. International Society for Optics and Photonics, p 113151F
36. Ong RE, Ou JJ, Miga MI (2010) Non-rigid registration of breast surfaces using the laplace and diffusion equations. Biomed Eng Online 9 (1):8
37. Fitzpatrick JM, Hill DL, Maurer Jr CR (2000) Image registration. Handbook of Medical Imaging 2:447-513
38. I ND (2020) Polaris Vicra - NDI. Northern Digital Inc. https://www.ndigital.com/products/polaris-vicra/. Accessed June 2 2021 2021
39. Chan S, Chen J-H, Li S, Chang R, Yeh D-C, Chang R-F, Yeh L-R, Kwong J, Su M-Y (2017) Evaluation of the association between quantitative mammographic density and breast cancer occurred in different quadrants. BMC cancer 17 (1):274
40. Darbre PD (2005) Recorded quadrant incidence of female breast cancer in Great Britain suggests a disproportionate increase in the upper outer quadrant of the breast. Anticancer Res 25 (3C):2543-2550
41. Lee AH (2005) Why is carcinoma of the breast more frequent in the upper outer quadrant? A case series based on needle core biopsy diagnoses. Breast 14 (2):151-152
42. DeSantis CE, Ma J, Gaudet MM, Newman LA, Miller KD, Goding Sauer A, Jemal A, Siegel RL (2019) Breast cancer statistics, 2019. CA Cancer J Clin 69 (6):438-451
43. Mango V, Ha R, Gomberawalla A, Wynn R, Feldman S (2016) Evaluation of the SAVI SCOUT surgical guidance system for localization and excision of nonpalpable breast lesions: a feasibility study. AJR Am J Roentgenol 207 (4):W69-W72
44. Sharek D, Zuley ML, Zhang JY, Soran A, Ahrendt GM, Ganott MA (2015) Radioactive seed localization versus wire localization for lumpectomies: a comparison of outcomes. AJR Am J Roentgenol 204 (4):872-877